Chemical Geology 450 (2017) 145–153

Contents lists available at ScienceDirect

Chemical Geology

journal homepage: www.elsevier.com/locate/chemgeo

Publisher's note

The effect of growth rate on uranium partitioning between individual calcite crystals and fluid

Jeremy M. Weremeichik [a,*,1], Rinat I. Gabitov [a], Bruno M.J. Thien [b], Aleksey Sadekov [c]

[a] Mississippi State University, MS 39762-5448, USA
[b] Paul Scherrer Institut, Laboratory for Waste Management, Switzerland
[c] University of Cambridge, Cambridge CB23EQ, UK

ARTICLE INFO

Article history:
Received 19 July 2016
Received in revised form 17 December 2016
Accepted 19 December 2016
Available online 22 December 2016

Keywords:
Calcite
Uranium
Partition coefficient
Growth rate
SIMS
Disequilibrium

ABSTRACT

Elemental to calcium ratios in calcium carbonate minerals are used to study environmental conditions. In particular, uranium to calcium ratio (U/Ca) has been proposed as a proxy for seawater carbonate ion concentration (CO_3^{2-}) and seawater pH. This work is focused on the evaluation of growth rate and its effect on uranium partitioning between calcite and fluid. We grew inorganic calcite (by diffusion of CO_2) isothermally from NH_4Cl-$CaCl_2$ doped with uranium. The growth rate of calcite (crystal extension rate, V) was monitored by sequentially spiking calcite-precipitating fluids with rare earth element (REE) dopants. The REE was analyzed with secondary ion mass spectrometry (SIMS) at spots matching those where U/Ca was determined. Partition coefficient $K^U = (U/Ca)_{calcite} / (U/Ca)_{fluid}$ increases with increasing growth rate (V). Specifically, K^U increases from 0.02 to 0.06 when V increases from 0.01 to 0.14 nm/s and remains nearly constant at faster rates. Numerical simulations using the growth entrapment model (GEM) and unified uptake kinetics model (UUKM) were undertaken to explain K^U-V relationship in the recent data on calcite.

1. Introduction

Uranium is a trace element commonly present in calcium carbonate minerals found in both marine and terrestrial environments (e.g. Reeder et al., 2001; Dunk et al., 2002; Kelly et al., 2003, 2006). The presence of uranium in calcite is of value to the geological community as it is utilized in U-series age-dating as a geochronological tool (e.g. Lundberg and Ford, 1994; Ku et al., 1998; Kelly et al., 2006). Through the preservation of its signature in calcite, the U/Ca ratio is being used to track geologic events, climatic variations, and the ocean uranium budget (e.g. Russell et al., 1994; Min et al., 1995; Dunk et al., 2002). Russell et al. (1994) investigate the applicability of U/Ca ratios in foraminiferal calcite as a proxy for seawater uranium concentrations. Min et al. (1995) discover annual variations in the U/Ca ratio coral skeletons and that U/Ca is inversely correlated with measured temperatures which suggest it has potential as a paleothermometer. Dunk et al. (2002) provide a new assessment of the pre-anthropogenic ocean uranium budget for the Holocene.

It is known from the work of Russell et al. (2004) and supported by the findings of Keul et al. (2013) that U/Ca ratios in foraminiferal calcite decrease by 25 ± 7% per 100 μmol kg-sw^{-1} as [CO_3^{2-}] in seawater increases from 110 to 470 μmol/kg. This is because uranium easily reacts with aqueous carbonate species, and therefore speciation is dependent on available [CO_3^{2-}] in seawater (Keul et al., 2013). Moreover, as the abundance of the carbonate ion increases the diversity of uranium-carbonate complexes increases (e.g. [$UO_2(CO_3)_{(aq)}$], [$UO_2(CO_3)_3^{4-}$], and [$UO_2(CO_3)_2^{2-}$]) (Keul et al., 2013). Chemical speciation calculations were performed by Keul et al. (2013) using the Visual Minteq ver. 3.0 software (Gustafsson, 2010). As the sum of the different carbonate complexes increases the percentage of free forms [UO_2^{2+}] and [$UO_2(CO_3)_2^{2-}$] decreases (Keul et al., 2013). In addition to the findings of Keul et al. (2013) it was reported by Dong and Brooks (2006) that [$UO_2(CO_3)_3^{4-}$] (>99%) is the predominate uranium species with trace amounts of [$UO_2(CO_3)_2^{2-}$] under experimental settings where the [CO_3^{2-}] concentration is high. These findings with those of Djogić et al. (1986) that the most dominate species is [$UO_2(CO_3)_3^{4-}$] with trace amounts of [$UO_2(CO_3)_2^{2-}$].

In addition, U/Ca has been proposed for determining paleo-pH, using coral skeletons and polyps, respectively (Min et al., 1995; Inoue et al., 2011; Raddatz et al., 2013); and ocean redox chemistry proxies using foraminiferal coatings (Boiteau et al., 2012). Foraminiferal coatings are produced by authigenic uranium within pore waters accumulating on the foraminiferal shell. It was shown by Inoue et al. (2011) that as pH increases, the U/Ca ratio decreases in skeletal coral polyps by −1.5 ± 0.2%

* Corresponding author.
E-mail address: jweremeichik@csc.edu (J.M. Weremeichik).
[1] Present address: Chadron State College, Chadron, NE, 69337 USA.

http://dx.doi.org/10.1016/j.chemgeo.2016.12.026
0009-2541/

change per 0.1 pH unit. During the glacial periods, the U/Ca ratios increased by nearly 50 to 250 nmol/mol for foraminiferal species *G. bulloides*, *G. inflata*, and *Uvigerina* spp. (Boiteau et al., 2012).

It was shown that U/Ca is heterogeneous in calcite grown at near-constant temperature, pH, Eh, and fluid composition (e.g. Reeder et al., 2001; Raitzsch et al., 2011). In Sturchio et al. (1998), it was demonstrated that the distribution of uranium in calcite is heterogeneous by conduction of X-ray fluorescence mapping. To better understand the heterogeneous distribution of uranium in calcite, this study seeks to evaluate crystal growth rate effect on the partitioning of uranium between calcite and fluid.

The strong influence of growth rate on partitioning of divalent cations, sulfate, and borate between calcite and fluid has been reported by several authors (e.g. Lorens, 1981; Busenberg and Niel Plummer, 1985; Tesoriero and Pankow, 1996; Gabitov and Watson, 2006; Lakshtanov and Stipp, 2007; Tang et al., 2008a; Saulnier et al., 2012; Mavromatis et al., 2013; Gabitov et al., 2014a). Uranium is different from the aforementioned elements due to the presence of various aqueous chemical species which occur in natural fluids at environmental conditions (e.g. Djogić et al., 1986; Reeder et al., 2001; and references therein). Uranium partitioning data are restricted to the work of Kitano and Oomori (1971) where the calcite growth rate was not determined and K^U was found to vary between 0.0n to 0.2. Although no definition of "n" was observed in their paper, we presume "n" stands for an integer. K^U can be described as the partition coefficient of uranium between calcite and fluid where $K^U = (U/Ca)_{calcite} / (U/Ca)_{fluid}$. Another group which looked at uranium partitioning was Meece and Benninger (1993), though the precipitation of both calcite and aragonite in many of their experiments complicates the applicability of their work to this study.

This work is concerned with the dependence of K^U on the crystal extension rate as evaluated in individual calcite crystals. The choice of $K^U = (U/Ca)_{calcite} / (U/Ca)_{fluid}$ instead of $K^U = (U/CO_3)_{calcite} / (U/CO_3^{2-})_{fluid}$ was based on the lack of CO_3^{2-} data for experimental fluids during early crystallization and the wide use of U/Ca in studying of natural calcium carbonates. Growth rate values for this study were determined in-situ as the width of the layers of calcite divided by growth time of each calcite zone (e.g. Gabitov et al., 2012). Each calcite zone was identified using SIMS analysis by the presence of specific rare-earth elements (REEs) which were added to the growth medium at distinct time intervals.

To explain the obtained experimental data, we conducted quantitative simulations using growth entrapment (GEM) and unified uptake kinetics (UUKM) models after Watson (2004) and Thien et al. (2014), respectively. Elemental partitioning between mineral and fluid is not a constant value; when K is predicted by thermodynamics (i.e. K at equilibrium) it corresponds to K measured at very low growth rate. In contrast disequilibrium K values are being measured in rapidly grown calcite. Several models have been developed to account for this non-equilibrium uptake of trace elements in growing minerals. The UUKM (Thien et al., 2014) is based on the two models developed by Watson (2004) and DePaolo (2011), but is implemented in the GEM-Selektor V3 geochemical modeling package (Kulik et al., 2013). The utilization of the UUKM allows the user to account for solution changes (e.g. depletion) which can influence the growth rates and therefore the value of K.

2. Experimental and analytical methods

2.1. Calcite precipitation

The calcite growth method used here was based on early works of Gruzensky (1967) and Paquette and Reeder (1995) but was modified by the introduction of sub-sampling and multiple REE spikes. Additional details regarding the experiment are described in previous works of Gabitov et al. (2012, 2014a, 2014b). The calcite growth medium was prepared by dissolving NH_4Cl in deionized (DI) H_2O to the concentration of 0.5 mol/l, along with minor amounts of reagent grade $CaCl_2 \cdot 2H_2O$ (0.01), $MgCl_2 \cdot 6H_2O$ (10^{-3}), $SrCl_2 \cdot 6H_2O$ (10^{-4}), $BaCl_2 \cdot 2H_2O$ ($2 \cdot 10^{-5}$), $LiOH \cdot H_2O$ ($5 \cdot 10^{-4}$), H_3BO_3 (0.01), and U ICP-MS standard (10^{-5}) [values in parentheses are concentrations in mol/l]. ICP-MS standard consisted of 1000 ppm of U dissolved in 2% HNO_3. The pH of the solution was initially adjusted to 5.5 by the addition of reagent grade NaOH to match the pH from the study of Paquette and Reeder (1995). Calcite grew in a seedless Ca-bearing fluid with an initial volume of two liters (run DC-1, Pyrex® flask, slow growth) and 1.0 l (run DC-3, polypropylene container, fast growth) by diffusion of CO_2 (and NH_3) from slowly decomposing ammonium carbonate. Within the growth vessel a piece of ammonium carbonate (a few cm^3 in volume) was allowed to diffuse into a head space of about 200 ml at the beginning of the experiment (Fig. 1). The head space increased over the duration of the experiment to 700 ml due to the collection of fluid samples during slow calcite growth experiment. This method yielded growth of large crystals (>1 mm in size) without stirring of the fluid. Mixing was applied after addition of each REE spike by repeated injection and withdrawal of fluid using a 60-ml syringe. REE spikes (Sm, La, Nd, Tb, and Pr) were sequentially introduced into the growth medium in the amount of 1 ml of diluted REE-bearing solution after 24, 36, 86, and 129 days (t_{REE}) respectively, counting time from the addition of Sm ($t_{Sm} = 0$) (Table 1). After removal of fluid, flask was rinsed with DI water and crystals were detached from the inner walls of the flask with spatula. Only one crystal was measured. However, other cations (i.e. Mg and Sr) and oxygen isotopes yielded similar distribution within individual crystals (Gabitov et al., 2012; Gabitov et al., 2014a). The entire time of calcite precipitation was 150 days. The fluids were sampled periodically for measurement of pH and stored in a refrigerator for future use. The pH (NBS-scale) was measured immediately after collection of the fluid using an OAKTON pH 510 meter with "All-in-One" pH/Temp electrode calibrated with 7.00 and 10.00 pH buffers stored at the same temperature as the experiments. The fluid pH increased slowly during calcite precipitation from 7.96 ± 0.06 to 8.17 ± 0.02

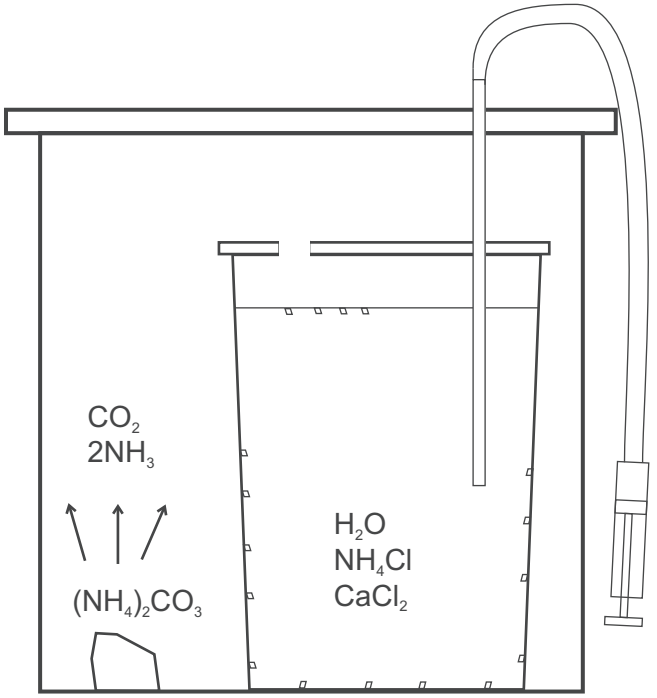

Fig. 1. Experimental setup for the coprecipitation of uranium with calcite by CO_2 diffusion technique developed by Gabitov et al. (2012) and described in Gabitov et al. (2014a, 2014b). An atmosphere, elevated with respect to $CO_{2(g)}$ and $NH_{3(g)}$, in the outer container diffuses with the Ca-enriched fluid – in the inner polypropylene (or Pyrex glass) container – through the opening in the lid. The diffusion induced precipitation of calcite can be expressed by the equation: $Ca^{2+} + CO_2 + OH^- = CaCO_3 + H^+$.

Table 1
Composition of the sampled fluids in DC-1 and DC-3 experiment.

Sub-sample	t days	U/Ca mmol/mol	1σ	pH	DIC μmol/kg	CO_3^{2-} μmol/kg	Ω
Slow growth run							
DC-1							
Initial	-43	0.919	0.065	5.5	low	low	low
Nd-spike	36	0.786	0.055	8.06	2410	170.2	1.95
Tb-spike	86	1.18	0.084	8.15	2685	229.9	2.40
Final	150	1.66	0.117	8.17	2775	247.8	1.71
Fast growth run							
DC-3							
Initial	-2.71	0.946	0.067	7.59	–	–	–
Sm-spike	0	1.13	0.080	7.83	–	–	–
Nd-spike	2.17	3.99	0.282	7.88	–	–	–
	4.17	8.76	0.619	7.91	–	–	–
Final	14.06	26.5	1.874	8.13	–	–	–

Initial solution is the same for all experiments.
t is the time of crystallization from the addition of Sm spike. Initial time was estimated as 43 days prior Sm addition by visual monitoring of the experimental flask with naked eye every 1–2 days.
Sm, Nd, and Tb correspond to the fluid sub-sample collected just before addition of REE.
pH of the fluid at the onset of crystallization was estimated to be 7.96 ± 0.06, which is the average of pH values at $t = -8$ and $t = 0$ days. See Fig. S-1 in Gabitov et al. (2012) for the whole pH record.
CO_3^{2-} and Ω calculations were performed using an excel implementation of CO2SYS (Lewis and Wallace, 1998), modified to use measured calcium concentrations. The constants of Millero (1995) were used for the carbonate and sulfate system, respectively. Salinity (S) of 29.4‰ was estimated by the amount of salts added into the initial fluid. The solubility product of calcite (K_{sp}^*) was calculated using the expression developed by Mucci (1983), yielding pK_{sp}^* of 6.46. The analytical + dilution errors for U and Ca are 5% and were used to calculate error for U/Ca. DIC was not measured for fast growth run DC-3.

(Table 1). Oxygen reduction potential was measured in a similar experiment and yielded oxidation conditions with an Eh of 0.127 V. These measurements were made using a Hanna Instruments HI5521-01, SN: D0079301 equipped with a refillable combination oxidation reduction potential (ORP) electrode HI3131B which was calibrated using HI7021 240 mV ORP solution and HI7022 470 mV ORP solution.

2.2. Analyses of fluids

Elemental analyses of the fluids were performed using Thermo Element XR, ICP-MS at the University of Cambridge (UK), Department of Earth Sciences with the precision of 5% (1σ). Dissolved inorganic carbon (DIC) was determined using the coulometric SOMMA (Single-Operator Multi-Metabolic Analyzer) system in the Biogeochemistry Laboratory at UCLA with an accuracy of ±2.1 μmol/kg (for details see Johnson et al., 1993).

2.3. In-situ analyses of calcites

XRD analyses and microscopy confirmed the precipitated phase was calcite. The crystals of the largest sizes were mounted in epoxy (EpoxiCure®, Buehler) such that the pyramid base (the crystal side adjacent to the substrate during growth) was exposed for SIMS measurements. The mounts were polished with Buehler SiC paper of 400, 600, 800, and 1200 grit following by 1-μm size diamond paste. SIMS analyses were conducted with CAMECA ims 1270 ion microprobe at UCLA (USA), first to determine REE/Ca, and next to evaluate U/Ca. REE/Ca analysis is described in Gabitov et al. (2012). Briefly, individual crystals were analyzed with a 3–18 nA $^{16}O^-$ primary beam at 20–30 μm lateral dimension on the sample surface. Positive secondary ions corresponding to mass/charge stations of 41.7 (background), ^{42}Ca, 87.5 (background), ^{88}Sr, ^{139}La, ^{141}Pr, ^{143}Nd, ^{149}Sm, and ^{159}Tb were measured (see Gabitov et al., 2012 for details). To reduce molecular interferences of Sr^{2+} and REE molecular species, Ca and REE were analyzed with a sample voltage offset of −60 eV, and using the energy bandwidth of 50 V (total voltage was 10 keV). It was shown that energy filtering reduces molecular interferences during measurements of ^{42}Ca and ^{88}Sr from carbonate materials down to 0.3% using different ion probes including ims-1270 (Herzog et al., 1973; Shimizu et al., 1978; Allison, 1996; Hart and Cohen, 1996; Denniston et al., 1997; Gaetani and Cohen, 2006; Monteleone et al., 2007; Gabitov et al., 2013). REEs were analyzed for identification of spiked REE zones only.

U/Ca analysis was conducted at X-Y coordinates similar to those in REE analysis. U/Ca analytical profiles 1 and 2 correspond to REE/Ca profiles 4 and 5 reported in Gabitov et al. (2014a). ^{42}Ca and ^{238}U were collected within 10 cycles using axial electron multiplier. To reduce molecular interferences of Sr^{2+} Ca was analyzed with a sample voltage offset of −60 eV, and using the energy bandwidth of 50 V (total voltage was 10 keV); no energy offset was applied for U measurements. The reproducibility was first tested on NIST-612 glass where 1 s.d. of $^{238}U/^{42}Ca$ was 1.2% between 9 spot analyses during the analytical session. The chemical match between standard and unknown is required to minimize instrumental mass fractionation in SIMS analyses, therefore, reference calcite LAS-20 was used for evaluation of U/Ca in our sample. The reference value for U/Ca in LAS-20 (U/Ca 119.3 ± 7.4 μmol/mol) was adopted from ICP-MS data reported in Table 1 of Sano et al. (2005).

Twenty-five spot analyses of LAS-20 yielded standard deviation (1 s.d.) of 23.5%, which was reduced to 9.0% after removal of three outlier data, where uranium contents were lower than the average value by factors of two and ten (see appendix). No correlation between backscattered electron intensities collected with scanning electron microscopy and U/Ca SIMS data was evaluated. Our reproducibility value (1 s.d. = 9.0%) is consistent with that found in the literature on LAS-20 data collected by ICP-MS, LA-ICP-MS, and Nano-SIMS; where 1σ = 6.2%, 9.8%, and 13.4% respectively (Sano et al., 2005).

2.4. Geochemical simulations

Two models GEM (Watson, 2004) and UUKM (Thien et al., 2014) were applied to explain uranium partition data, which cannot be modeled using thermodynamics only. The above-mentioned models consider deviation of trace element concentration from equilibrium. The GEM – or, as it is referred to by Thien et al. (2014), Surface (growth) Entrapment Model – accounts for the distribution of trace elements upon incorporation into the crystal lattice once it has been buried beneath the surface. The GEM assumes crystal growth from uniform and infinite reservoir. The UUKM is a unified model which incorporates both the GEM and Surface Reaction Kinetics Model (SRKM) (DePaolo, 2011), which is based on the dynamics of precipitation-dissolution reactions at the crystal surface. In addition, the UUKM predicts changes in the composition of fluid and speciation throughout the course of an experiment. The SRKM model is based on the dynamics of precipitation-dissolution reactions at the crystal surface.

2.4.1. Simulation using the growth entrapment model (GEM)

Simulations were conducted using a new version of the GEM code (GEM2) running with QB64. The model presented here is based upon the work of Watson and co-workers (Watson, 1996; Watson, 2004; Watson and Liang, 1995) and the successful use of the model (Stoll et al., 2002; Gaetani and Cohen, 2006; Tang et al., 2008a, 2008b; Gabitov et al., 2008; Gabitov et al., 2014b). The model can be described by the following relationship:

$$C(x) = C_{eq} \cdot F^{\exp(x/1)} \quad (1)$$

where $C(x)$ is the concentration of uranium in the crystal at some distance x from the surface, C_{eq} is the concentration reflecting the equilibrium partitioning of uranium between the growth medium and the crystal lattice, F is the surface enrichment factor, and l (0.5 nm) is the half-thickness of the enriched surface layer. The choice of 0.5 nm was based on successful application of GEM in fitting of experimental data on cation partition coefficients versus crystal growth rate (e.g. Watson, 2004; Gaetani and Cohen, 2006; Tang et al., 2008a, 2008b).

The surface enrichment factor was calculated using the following equation:

$$F = (C_s/C_{eq}) = (K_s/K_{eq}) \quad (2)$$

where C_s is the concentration of uranium in the surface layer of calcite, K_s is the partition coefficient between surface layer and fluid, i.e. the U/Ca ratio at the surface of the crystal divided by the U/Ca ratio measured in the fluid, K_{eq} is the equilibrium partition coefficient of uranium which is equal to the U/Ca ratio at equilibrium in the lattice (by considering an aqueous-solid solution between calcite, $CaCO_3$, and the mineral rutherfordine, UO_2CO_3) divided by the U/Ca ratio of the fluid. The definition of K_{eq} we considered is:

$$K_{eq} = \frac{\left(x_{Rutherfordine}/x_{Calcite}\right)}{\left(a(U^{VI})/a(Ca^{II})\right)} \quad (3)$$

where x are solid molar fractions, and a are the aqueous activities. In the consideration of experimental conditions (i.e. fluid composition, Eh, pH, temperature), the aqueous concentration of Ca^{II} is nearly equal to the total dissolved Ca; the aqueous concentration of all the U(VI) species is practically equal to the total concentration of dissolved uranium. It is, therefore, more convenient to use total dissolved concentrations in Ca and U, especially when pH of the fluid changes within an individual or between different experiments. The GEM calculates K^U as a function of V with a complex differential equation that is mathematically derived from (Eq. 1), as described in Thien et al., 2014.

2.4.2. Simulation using the unified uptake kinetics model (UUKM)

Additional efforts were undertaken by running simulations using the UUKM. This model is combined with the GEM-Selektor v.3 geochemical modeling package (Wagner et al., 2012 and Kulik et al., 2013). The entrapment in the UUKM can be described by the following equation:

$$K = \frac{F \cdot K_{eq}}{1 + \frac{D}{D+V} \cdot (F-1)} \quad (4)$$

This equation reports that K varies between 2 limits, as a function of the growth rate: K_{eq}, and $F \cdot K_{eq}$ which corresponds to the composition of the surface layer, controlled by sorption mechanisms. Co-precipitation experiments carried out at larger growth rate range are necessary for robust evaluation of K_{eq} and F. The surface diffusivity parameter D (nm^2/s) can be fitted if no relevant experimental data is available. The linear growth rate (i.e. extension rate of individual crystal) V, was recalculated at each time-step by using a kinetic equation modified from Wolthers et al. (2012). More explanations about this equation and its implementation in GEM-Selektor v.3 are provided in Thien et al. (2014).

The GEM-Selektor v.3 calculates the activities of the different aqueous species and complexes, and mineral phases, at each calculation step. The chemical thermodynamic system was set up for B, Ba, C, Ca, Cl, H, Li, Mg, N, Na, O, Sr, charge, assuming the overall charge neutrality. The list of components, species and phases used in the calculations and their corresponding thermodynamic data come from the Nagra-PSI database (Hummel et al., 2002). Aqueous activity coefficients calculations were done by using the extended Debye-Hückel equation with the common ion size parameter of 0.372 nm. The solid-solution between rutherfordine and calcite was added in the database. It includes the standard thermodynamic properties of the two end-members (i.e. rutherfordine and calcite), and an interaction parameter (i.e. non-ideality). The solubility of the two end-members depends on their respective thermodynamic properties, as well as the interaction parameter of the solid-solution. We adjusted the interaction parameter so that the results would fit with the experimental data. More details about solid solutions and their implementation in GEM-Selektor v.3 are given in Kulik et al. (2010) and Wagner et al. (2012).

The entrapment equation (see Eq. 4) is implemented as a process simulation script in GEM-Selektor v.3, and a precipitation kinetic equation of the considered mineral which provides the value of V for calcite (Wolthers et al., 2012). In the GEM, the mineral growth rate (V) is an input parameter; in the UUKM it is recalculated at each time step as a function of the solution composition.

The GEM predicts K as a function of the mineral growth rate assuming constant reservoir composition, so no long-term prediction of mineral composition can be obtained because the solution in a closed medium might be subject to depletion effects. The UUKM is more complex to use because it requires input in regards to the set-up of the chemical system, but after having circumvented this difficulty, it predicts the whole-time evolution of the system: mineral growth rate, mineral composition, and solution composition.

3. Results

3.1. Composition of fluids

Over the course of the experiment, Ca concentrations in the solution decreased from 307.6 ± 15.4 ppm to 110.9 ± 5.5 ppm (see Fig. 2a). It is important to note that $t = 0$ in Fig. 2 (a, b) denotes the time at which crystallization within the solution was first observed and Sm was introduced. U/Ca evolution is presented in Fig. 2b, which demonstrated the following fluid U/Ca relationship with respect to time (t) in days:

$$\begin{aligned} U/Ca\ (mmol/mol) &= 4 \cdot 10^{-5} \cdot t^2 - 2 \cdot 10^{-4} \cdot t + 8.19 \cdot 10^{-1} \pm 1.82 \cdot 10^{-3}, \quad R^2 \\ &= 0.97, \quad y\text{-intercept} = 9.09 \cdot 10^{-1} \pm 1.66 \cdot 10^{-1} \end{aligned} \quad (5)$$

The initial fluid had low DIC and CO_3^{2-}, which increased to an unknown value before the onset of crystallization. After that, DIC and CO_3^{2-} increased by 13 and 31% between 36 and 150 days after precipitation started (Table 1).

3.2. SIMS data

A SIMS profile was preformed which spanned the crystal (see Fig. 2c). The profile for which the data was collected is referred to as SIMS profile-1 and data related to the profile can be found in Table 2. SIMS analyses identified the crystal zones marked with REE, in which the appearance corresponds to the sequence of REE addition to the fluid (see Fig. 3). The growth rates were determined by the width of each zone (Δx) in each SIMS profile divided by the time between REE spikes (Δt). Determined V values showed that crystals grew fast in their interior slowing down toward the edges, i.e. V decreased from 0.1 to 0.01 nm/s in the Sm-La and Tb-Pr zones, respectively (Table 3). Scattered U/Ca ratios increase from the edge toward the center of slow (run DC-1) and fast growing (run DC-3) calcite crystals. It is important to note that the DC-3 crystal grew prior to the addition of 1-st REE spike. Therefore, the averaged value of U/Ca was used to calculate K^U for this profile. The variability of the U/Ca ratios in mmol/mol are presented in Table 2 and can be seen in Fig. 2. The SIMS analysis for the crystals was performed as profiles where the sampling distance, (L) in μm, ranges from 65 to 1729 μm for profile-1, 15 to 1284 μm for profile-2 and 40 to 603 μm for the DC-3 profile as a function of the sampling distance from the edge of the crystal (Table 2). The topography of individual crystals and standard grains was measured with interference microscope (PHASE SHIFT MicroXAM Surface Mapping Microscope Crystal). The results suggest that observed U/Ca trend in calcite samples is not an analytical artifact - i.e., observed U/Ca is not the result of <1 μm relief between center and edge of the crystals.

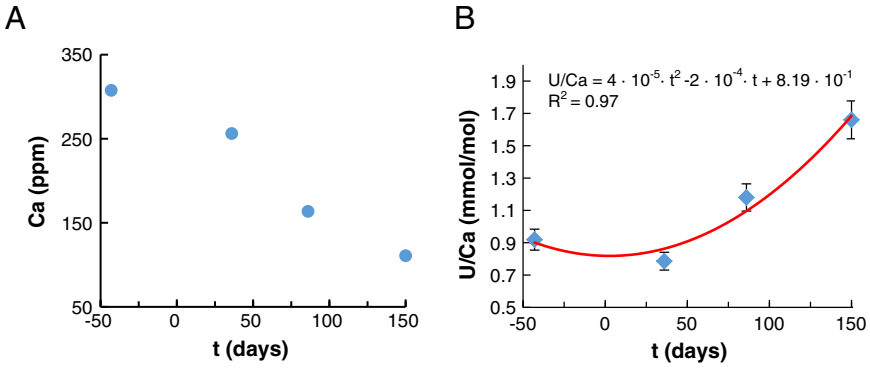

Fig. 2. Fluid and SIMS data. The evolution of Ca (a) and U/Ca (b) concentrations in solution throughout the duration of the experiment where (t) is the duration of the experiment and $t = 0$ is the time at which crystallization was first observed in the solution. Uranium concentration (mmol/mol) in a single calcite crystal.

3.3. Uranium partitioning data

The U/Ca calcite values show that as time increases the incorporation of uranium into calcite, in mmol/mol, decreases conversely to U/Ca in the fluid which increases with time (Table 3). Table 3 shows an elevated growth rate (V) during the first 36 days of growth for both slow growth profiles. The partition coefficient of uranium between calcite and fluid was calculated as $K^U = (U/Ca)_{calcite} / (U/Ca)_{fluid}$, where $(U/Ca)_{calcite}$ is defined as the averaged SIMS data from particular REE-spiked zones within the calcite. The uncertainty in $(U/Ca)_{calcite}$ was calculated as the standard error (1 s.e.) of the data from individual REE-spiked zone. $(U/Ca)_{fluid}$ was determined using Eq. (5). The error for growth rate is estimated as s.e. between V data from opposite sides of the crystal (Tables 2 and 3). In the fast precipitation run (DC-3) the data for each crystal were averaged as most of the crystal growth occurred before the addition of the first spike. K^U was determined from the average U/Ca between the initial fluid and when the Sm spike was added.

3.4. Modeling

By using GEM, modeling the experimentally measured values of K as a function of V (Fig. 4) implies an average value of K_{eq} of 0.02. This means that a small amount of uranium is incorporated with calcium carbonates at equilibrium. It is worth mentioning that Heberling et al. (2008) measured the same value of K for a calcite growth rate equivalent to 0.0025 nm/s. Regarding Fig. 4, such a growth rate is close to equilibrium, and this experimental result is therefore consistent with our simulation. To obtain the aforementioned result with the GEM Selektor code the user must input an interaction parameter of 1000 J/mol for the aqueous-solid solution between calcite and rutherfordine. The solution is slightly undersaturated with respect to rutherfordine. It nevertheless precipitates; when two minerals form a solid-solution their solubility's are less important than when one considers the single mineral's solubility. For more information regarding aqueous-solid solution we refer the reader to Kulik et al. (2010) and Wagner et al. (2012).

Table 2
SIMS analytical profiles of U/Ca.

L (μm) SIMS profile-1[a]	U/Ca (mmol/mol)	S.e.	L (μm) SIMS profile-2[a]	U/Ca (mmol/mol)	S.e.	L (μm) SIMS profile-DC-3	U/Ca (mmol/mol)	S.e.
65	0.0308	0.0023	15	0.0419	0.0021	40	0.0307	0.0021
94	0.0319	0.0016	55	0.0351	0.0025	90	0.0407	0.0028
130	0.0495	0.0032	95	0.0379	0.0025	140	0.0281	0.0013
174	0.0367	0.0017	155	0.0371	0.0024	190	0.0499	0.0018
219	0.0313	0.0014	215	0.0374	0.0019	240	0.0682	0.0027
264	0.036	0.0019	275	0.0389	0.0020	290	0.0775	0.0040
309	0.0371	0.0019	335	0.0416	0.0032	340	0.0638	0.0024
353	0.0432	0.0032	395	0.0369	0.0025	390	0.065	0.0030
398	0.0399	0.0035	455	0.0551	0.0028	440	0.0452	0.0017
443	0.0408	0.0016	945	0.0518	0.0033	490	0.0337	0.0017
493	0.0599	0.0031	1005	0.0388	0.0026	540	0.0365	0.0015
537	0.0561	0.0025	1065	0.0443	0.0017	603	0.0133	0.0014
591	0.0405	0.0016	1128	0.0260	0.0018			
1140	0.0495	0.0032	1189	0.0471	0.0022			
1183	0.0541	0.0019	1239	0.0376	0.0015			
1225	0.0467	0.0025	1284	0.0396	0.0023			
1267	0.0451	0.0017						
1310	0.048	0.0021						
1352	0.0435	0.0023						
1395	0.0507	0.0031						
1437	0.0486	0.0022						
1480	0.0456	0.0026						
1522	0.0388	0.0019						
1564	0.0352	0.0019						
1607	0.0285	0.0021						
1649	0.0257	0.0017						
1689	0.0449	0.0032						
1729	0.0385	0.0016						

SIMS analyses were performed as profiles between the edges of the crystals. For example distance L of 65 and 1729 μm corresponds to the opposite edges of the crystal, i.e. start and end of analytical profile. S.e. of U/Ca is the standard error at 1σ level which consists of the single spot s.e. (n = 10) and s.e. from multiple analyses on LAS-20 reference material (n = 20).

[a] Growth rate data are from Gabitov et al. (2014a) (DC-1 Crystal-1 profile-4 and profile-5 respectively).

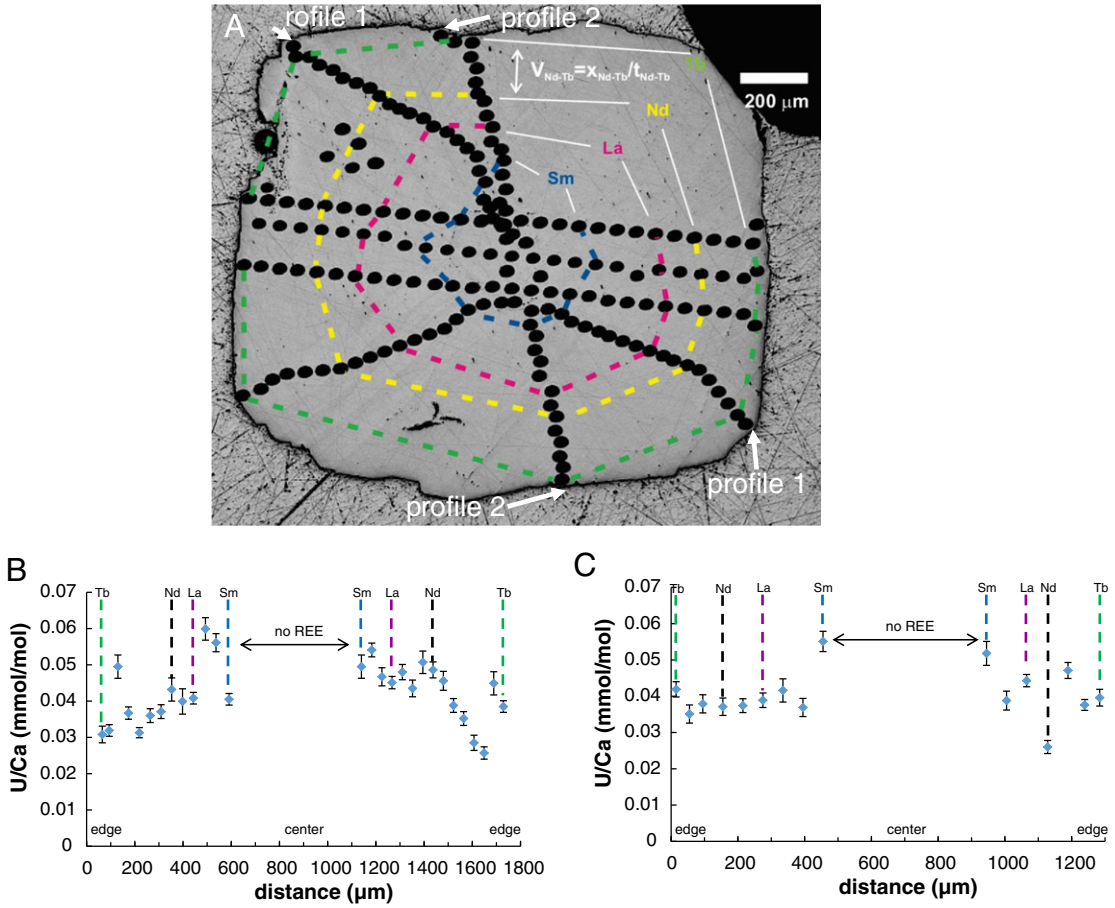

Fig. 3. (a) Optical microscopy image(s) of a calcite crystal from this study and Gabitov et al. (2012 and 2014a, b). The image was collected after SIMS analysis to determine REE/Ca ratios. The black spots are burn-marks from the six analytical profiles. SIMS profile-1 (b) and profile-2 (c) were performed on a single crystal in which the profiles span the crystal (SIMS profile-1 and profile-2, see Table 1.). No REE indicates the zone of crystal growth before the injection of any REEs to the solution. It also indicates the area where SIMS analysis was not conducted for this profile. The labels 'Sm, La, Nd, Tb' are makers which show when each REE-spike was added to the solution.

Based on the discussion of Eq. (1) outlined above, *F* (surface enrichment factor) was found to be 3. The numerical simulation of the growth rate of calcite with incorporated uranium can be seen in Fig. 4. To achieve the desired fit while using the GEM a multiplier parameter (m) was used. This multiplier parameter was set to infinity which implies that diffusivity is equal to diffusion in the near-surface region (D_s) at the distance much greater than the thickness of the near-surface layer. This is because in the model when the value of diffusivity in the calcite lattice (D_l) is much less than D_s the value of D_l becomes less important to the model. To fit experimental data, D_s was adjusted to 0.01 nm^2/s. The value of obtained D_s is much higher than D_l which was assumed to be 10^{-18} nm^2/s based on the values used in previous work (i.e. Gabitov et al., 2014a) due to the lack of experimental data for uranium diffusion to calcite. To confirm that the value selected for

Table 3
U partitioning data.

REE	t days	V nm/s	V error	U/Ca calcite mmol/mol	S.e.	U/Ca fluid mmol/mol	S.e.	K^U	S.e.
Slow growth run DC-1, profile 1									
Tb-Pr	86-129	0.011	0.001	0.0337	0.0024	1.258	0.358	0.0268	0.0079
Nd-Tb	36-86	0.055	0.008	0.0381	0.0020	0.956	0.232	0.0398	0.0099
La-Nd	24-36	0.143	0.031	0.0466	0.0022	0.850	0.026	0.0549	0.0031
Sm-La	0-24	0.121	0.011	0.0503	0.0026	0.823	0.018	0.0611	0.0034
Slow growth run DC-1, profile 2									
Nd-Tb	36-86	0.040	0.004	0.0378	0.0193	0.956	0.232	0.0395	0.0098
La-Nd	24-36	0.089	0.006	0.0367	0.0038	0.850	0.026	0.0431	0.0047
Sm-La	0-24	0.086	0.010	0.0445	0.0055	0.823	0.018	0.0540	0.0067
Fast growth run DC-3									
Sm	0	≥1.8	n/a	0.0509	0.0053	1.024	0.209	0.0497	0.0114

Growth rate data are from Gabitov et al. (2014a) (Table 2: slow growth run DC-1, Crystal-1, profile 4; slow growth run DC-1, Crystal-1, profile 5; Fast growth run DC-3, Cr1).
U/Ca in calcite is the average of a few spot analyses in particular REE spiked zones; s.e. (1σ) is the standard deviation of multiple spots divided by the square root of the number of spots (n) in each REE spiked zone. n varies from 3 to 6 in all REE-spiked zones except Tb-Pr zone, where n = 1.
In fast precipitation runs most of the growth occurred before the addition of 1st spike (Sm) therefore average U/Ca between initial fluid and Sm addition is considered in the run DC-3.
Error for growth rate is estimated as s.e. between two V data from the opposite sides of the crystal.

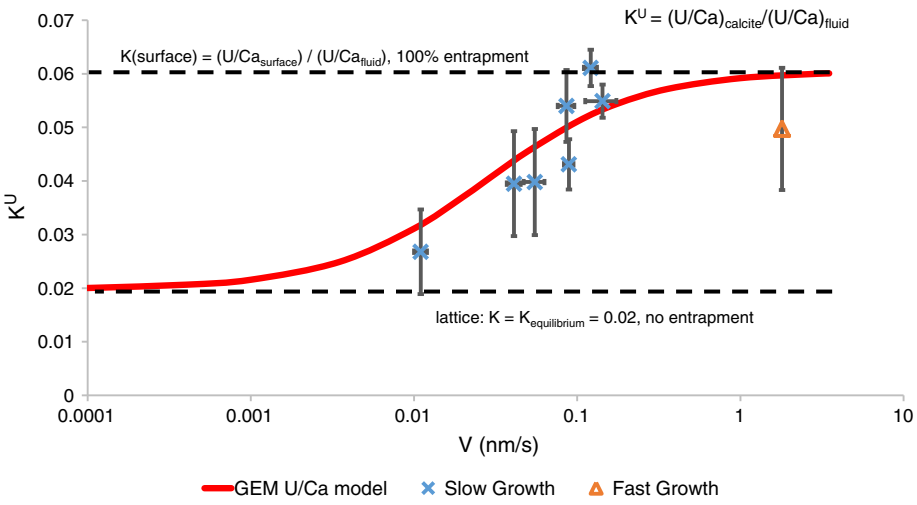

Fig. 4. Fractionation coefficient of U in calcite as a function of growth rate, V (nm/s). This graph presents the simulated data which was produced using the GEM software package. The growth rate data from Gabitov et al. (2014a) is also plotted on the graph to show that the synthetically produced calcite grew at near 100% entrapment. It is worth mentioning that Heberling et al. (2008) measured a similar value of K for a calcite growth rate equivalent to 0.0025 nm/s. The parameters F = 3, V = $1 \cdot 10^{-4}$ to 3.5, D_s = 0.01, $D_l = 1\ 10^{-18}$, l = 0.5, m = 600, and a K_{eq} = 0.02 were used to calculate the GEM model curve seen in this figure. Error for K^U was determined in the following manner $\sqrt{(\sigma_{U/Ca})^2/(U/Ca\ Fluid)^2 + (\overline{U/Ca})^2 \times (\sigma_{U/Ca\ Fluid})^2/(U/Ca\ Fluid)^4}$.

D_l does not affect the simulation results as far as $D_l << D_s$; simulations were run using a D_l of 10^{-44} nm^2/s which changed the K^U by 0.001%, which was far smaller than the minimum K^U error for SIMS analytical precision (5.6%, see Table 3). These findings agree with XPS works conducted by Stipp et al. (1992) and Hoffmann and Stipp (2001) and elaboration of Watson (2004) suggest that the diffusion of divalent cations in the near surface region of calcite is many orders of magnitude faster than in calcite lattice.

The UUKM input parameters were nearly identical to those used in GEM: K_{eq} = 0.02 and F = 3. D = 0.017 nm^2/s. This model provides the composition of the mineral as a function of the time (Fig. 5). It is important to note that when using the UUKM, the uranium speciation is nearly constant (i.e. *maximum* variation of 1% during the simulation) in that practically only two species appear (i.e. $CaUO_2(CO_3)_3^{2-}$ - 53% on average and $UO_2(CO_3)_3^{4-}$ - 45% on average). All the dissolved U species present in the system belong to the U(VI) group.

4. Discussion

The information provided by Fig. 4 suggests that 100% entrapment occurs at V > 1.0 nm/s at K^U of about 0.06 meaning that a maximum K^U is reached at V > 1.0. This is inconsistent with the data of Kitano and Oomori (1971) who observed a maximum K^U value of 0.2 at similar pH values. An explanation for the differences in the maximum K^U reported for the two studies most likely stems from the fact that Kitano and Oomori (1971) used a different definition for their partition coefficient ($K^{UO^{2+}}$). The partition coefficient used by Kitano and Oomori (1971) only considered UO_2^{2+} in their calculations whereas in our study we considered the total dissolved uranium concentration. The fact that UO_2^{2+} is not the major uranium species when pH > 6 (Djogić et al., 1986), mathematically implies that $K^{UO^{2+}}$ obtained by Kitano and Oomori (1971) are higher than those obtained in this study. Conversely, Meece and Benninger (1993) considered the same definition as this study and did not omit any species or complex during measurement because they measured radioactive activity. After having corrected for the effect of contaminating aragonite (calcite and aragonite do not have the same K^U values), they established a minimum value of K^U of about 0.046. For comparison, the growth rate range of the synthetic calcite produced in our study is 0.01–0.14 nm/s (0.86–12.10 μm/day). These values overlap with values reported for naturally occurring $CaCO_3$ ($3.13 \cdot 10^{-6}$–3.30 nm/s or $2.7 \cdot 10^{-4}$–285.12 μm/day) in benthic foraminifera (e.g. Ter Kuile and Erez, 1984), coccolithophorids (e.g. Stoll et al., 2002), scallops (e.g. Krantz et al., 1984; Owen et al., 2002), and speleothems (e.g. Baker et al., 1998; Genty et al., 2001; Winograd et al., 2006).

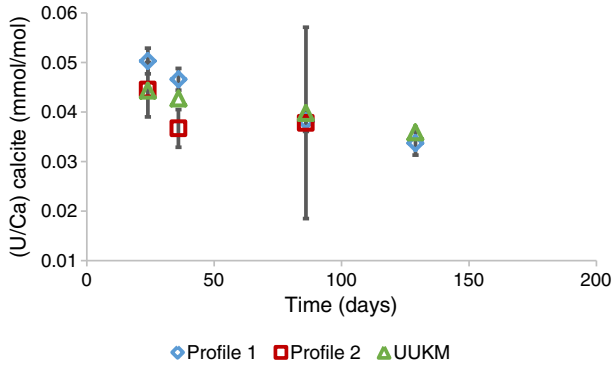

Fig. 5. The U/Ca ratio in calcite (mmol/mol) as a function of time. This graph presents the modeling results of UUKM in addition to the values presented in Table 3 for Slow growth run DC-1, profile 1 and 2 and Fast growth run DC-3.

The pH values reported in the experiments of Meece and Benninger (1993) (8.25 to 9) were higher than those reported for our experiments (8.0 to 8.2) and do not lead to a different speciation of U (Krestou and Panias, 2004). This phenomenon is exclusive to uranyl tricarbonate-like complexes in the presence of carbonates and similar U aqueous concentrations (Elzinga et al., 2004; Krestou and Panias, 2004). Nonetheless, in the experiments of Meece and Benninger (1993), the solution contains much more Mg (sea-water concentration) than in our experiments. According to the GEM-Selektor v.3., under the conditions achieved by Meece and Benninger (1993), $MgUO_2(CO_3)_3^{2-}$ becomes a dominant species with $CaUO_2(CO_3)_3^{2-}$ and $UO_2(CO_3)_3^{4-}$. We do not know if one of those species can be better incorporated or sorbed by calcite and at which pH, but excluding $MgUO_2(CO_3)_3^{2-}$ from the definition of K^U the value of K^U would not change >20%.

Both models – GEM and UUKM – can reproduce quantitatively the uranium incorporation in calcite we measured (Figs. 4 and 5). The GEM assumes uniform reservoir composition, which is not the case for our experiments, and therefore K^U instead of U/Ca was used for fitting with GEM. The UUKM accounts for the change of U/Ca in fluid providing

the absolute composition of the calcite. U/Ca for REE-spiked zones of calcite calculated with UUKM match U/Ca determined experimentally (Fig. 5) implying the ability of growth entrapment phenomena to explain uranium incorporation into calcite from a finite reservoir. High surface enrichment factors ($F > 1$) in calcite is consistent with F values proposed for Sr, Ba, and Se (Watson, 2004; Gabitov and Watson, 2006; Thien et al., 2014), suggesting a similar entrapment mechanism. However, the enrichment of uranium could be underestimated, thus, more experimental data at growth rates slower than in our experiments are necessary to determine K^U_{eq} and F values.

The partition coefficients that can be observed in Table 3 were calculated using K^U-CO_3^{2-} calibration for foraminifera (Keul et al., 2013). The values of CO_3^{2-} were calculated as averages between three sub-samples collected during the addition of Nd and Tb spikes and final fluid (200 and 239 μmol/kg for Nd-—Tb and Tb-final respectively). The obtained K^U values decrease from 0.129 to 0.108 with increasing of CO_3^{2-} from 200 to 239 μmol/kg, which is consistent with our data where K^U decreases from 0.040 to 0.027 (see Table 3, Nd-Tb and Tb-Pr spiked zones). However, absolute values of K^U are different by a factor of three. The low K^U in our work relative to foraminifera (Keul et al., 2013) and inorganically precipitated calcite (Meece and Benninger, 1993) could be explained by the difference in chemistry of our fluids and high uranium content (10^{-5} mol/l) whereas the uranium content in seawater is ~$1.5 \cdot 10^{-8}$ mol/l. It may also be possible that during biomineralization uranium is preferentially concentrated during DIC transport. For example, as foraminifers' uptake DIC, uranyl-DIC complexes may also be incorporated with calcifying fluid as part of this process. A third explanation proposed by Kelly et al. (2003) suggests that slowly grown natural calcites allow for an ordering of incorporated uranyl during growth whereas comparatively rapid grown synthetic calcites favor disordered incorporation of uranyl which may potentially explain the difference of the absolute values of K^U. More work is needed to clarify and isolate the cause of the depressed absolute K^U values.

5. Conclusions

It was shown for the first time that uranium incorporation in calcite increases with the growth rate of individual crystals. The phenomenon can be explained with the concept of growth entrapment proposed by Watson (2004). Though there are discrepancies between the current study and previously published values for maximum K^U (i.e. Kitano and Oomori, 1971) it has been determined that the minimum K^U value reported by Meece and Benninger (1993) is consistent with the K^U values of this study. A plausible explanation for the differences in the maximum K^U reported for the present study and that of Kitano and Oomori (1971) is that they used a different definition for their partition coefficient ($K^{UO^{2+}}$). To explore the provided explanation would require more experimental effort, especially on aqueous uranium species measurements. It was also demonstrated that both models (GEM and UUKM) fit the experimental data assuming similar equilibrium partition coefficient of uranium, its diffusivity in the near-surface region of calcite, and identical surface enrichment factor. This study provided an opportunity to show that the UUKM coupled with GEM-Selektor is able to predict trace element concentration in growing minerals when U/Ca in solution increased by the factor of two during the experiment.

Acknowledgments

We would like to thank the associate editor, Michael E. Böttcher and the reviewers, Axel Schmitt, Kevin McKeegan, and Mark Harrison for their help and support with the ion microprobe measurements. Experiments and SIMS analyses were supported by NSF, EAR, Instrumentation and Facilities Program grant no. 1029193. We are grateful to Mervyn Greaves and Harry Elderfield for support of elemental measurements at the University of Cambridge. We thank Anita Leinweber for measuring DIC; these analyses were covered by ETH grant no. 4 443869-AL-20600. Elemental measurements of the fluids were also covered by ERC grant NEWLOG 267931 to H. Elderfield. The development of the UUKM was made possible by the European Atomic Energy Community's Seventh Framework Programme (FP7/2007-2011) No. 269688. We thank Neil Sturchio for sharing the LAS-20 calcite. The authors are grateful to Bruce Watson for providing the code used to model growth entrapment.

References

Allison, N., 1996. Comparative determinations of trace and minor elements in coral aragonite by ion microprobe analysis, with preliminary results from Phuket, southern Thailand. Geochim. Cosmochim. Acta 60, 3457–3470.
Baker, A., Genty, D., Dreybrodt, W., Barnes, W.L., Mockler, N.J., Grapes, J., 1998. Testing theoretically predicted stalagmite growth rate with recent annually laminated samples: implications for past stalagmite deposition. Geochim. Cosmochim. Acta 62, 393–404.
Boiteau, R., Greaves, M., Elderfield, H., 2012. Authigenic uranium in foraminiferal coatings: a proxy for ocean redox chemistry. Paleoceanography 27.
Busenberg, E., Niel Plummer, L., 1985. Kinetic and thermodynamic factors controlling the distribution of SO_3^{2-} and Na^+ in calcites and selected aragonites. Geochim. Cosmochim. Acta 49, 713–725.
Denniston, R.F., Shearer, C.K., Layne, G.D., Vaniman, D.T., 1997. SIMS analyses of minor and trace element distributions in fracture calcite from Yucca Mountain, Nevada, USA. Geochim. Cosmochim. Acta 61, 1803–1818.
DePaolo, D.J., 2011. Surface kinetic model for isotopic and trace element fractionation during precipitation of calcite from aqueous solutions. Geochim. Cosmochim. Acta 75, 1039–1056.
Djogić, R., Sipos, L., Branica, M., 1986. Characterization of uranium(VI) in seawater. Liminol. Oceanogr. 31, 1122–1131.
Dong, W., Brooks, S.C., 2006. Determination of the formation constants of ternary complexes of uranyl and carbonate with alkaline earth metals (Mg^{2+}, Ca^{2+}, Sr^{2+}, and Ba^{2+}) using anion exchange method. Environ. Sci. Technol. 40, 4689–4695.
Dunk, R.M., Mills, R.A., Jenkins, W.J., 2002. A reevaluation of the oceanic uranium budget for the holocene. Chem. Geol. 190, 45–67.
Elzinga, E.J., Tait, C.D., Reeder, R.J., Rector, K.D., Donohoe, R.J., Morris, D.E., 2004. Spectroscopic investigation of U(VI) sorption at the calcite-water interface. Geochim. Cosmochim. Acta 68, 2437–2448.
Gabitov, R.I., Watson, E.B., 2006. Partitioning of strontium between calcite and fluid. Geochem. Geophys. Geosyst. 7, 1–12.
Gabitov, R.I., Gaetani, G.A., Watson, E.B., Cohen, A.L., Ehrlich, H.L., 2008. Experimental determination of temperature and growth rate effects on U^{6+} and Mg^{2+} partitioning between aragonite and fluid. Geochim. Cosmochim. Acta 72, 4058–4068.
Gabitov, R.I., Watson, E.B., Sadekov, A., 2012. Oxygen isotope fractionation between calcite and fluid as a function of growth rate and temperature: An in situ study. Chem. Geol. 306-307, 92–102.
Gabitov, R.I., Gagnon, A.C., Guan, Y., Eiler, J.M., Adkins, J.F., 2013. Accurate Me/Ca ratio measurements in carbonates by SIMS and nanoSIMS and an assessment of heterogeneity in common carbonate standards. Chem. Geol. 356, 94–108.
Gabitov, R.I., Sadekov, A., Leinweber, A., 2014a. Crystal growth rate effect on Mg/Ca and Sr/Ca partitioning between calcite and fluid: an in situ approach. Chem. Geol. 367, 70–82.
Gabitov, R.I., Rollion-Bard, C., Tripati, A., Sadekov, A., 2014b. In situ study of boron partitioning between calcite and fluid at different crystal growth rates. Geochim. Cosmochim. Acta 137, 81–92.
Gaetani, G.A., Cohen, A.L., 2006. Element partitioning during precipitation of aragonite from seawater: a framework for understanding paleoproxies. Geochim. Cosmochim. Acta 70, 4617–4634.
Genty, D., Baker, A., Vokal, B., 2001. Intra- and inter-annual growth rate of modern stalagmites. Chem. Geol. 176, 191–212.
Gruzensky, P.M., 1967. Growth of calcite crystals. In: Steffen Peiser, H. (Ed.), Crystal Growth, Conference Proceedings of the International Conference on Crystal Growth (1966: Boston MA)Supplement to Journal of Physics and Chemistry of Solids S: 365 Suppl. 1. Pergamon Press, New York.
Gustafsson, J.P., 2010. Visual MINTEQ, Version 3.00. KTH, Dept. Of Land and Water Resources Engineering, Stockholm, Sweden.
Hart, S.R., Cohen, A.L., 1996. An ion probe study of annual cycles of Sr/Ca and other trace elements in corals. Geochim. Cosmochim. Acta 60, 3075–3084.
Heberling, F., Denecke, M.A., Bosbach, D., 2008. Neptunium(V) coprecipitation with calcite. Environ. Sci. Technol. 42, 471–476.
Herzog, G.F., Anders, E., Alexander, E.C., Davis, P.K., Lewis, R.S., 1973. Iodine-129/xenon-129 age of magnetite from the orgueil meteorite. Science 180, 489–491.
Hoffmann, U., Stipp, S.L.S., 2001. The behavior of Ni^{2+} on calcite surfaces. Geochim. Cosmochim. Acta 65, 4131–4139.
Hummel, W., Berner, U., Curti, E., Pearson, F.J., Thoenen, T., 2002. Nagra/PSI Chemical Thermodynamic Data Base 01/01. Universal Publishers, Parkland, Florida.
Inoue, M., Suwa, R., Suzuki, A., Sakai, K., Kawahata, H., 2011. Effects of seawater pH on growth and skeletal U/Ca ratios of *Acropora digitifera* coral polyps. Geophys. Res. Lett. 38.
Johnson, K.M., Wills, K.D., Butler, D.B., Johnson, W.K., Wong, C.S., 1993. Coulometric total carbon dioxide analysis for marine studies: maximizing the performance of an automated gas extraction system and coulometric detector. Mar. Chem. 44, 167–187.

Kelly, S.D., Newville, M.G., Cheng, L., Kemner, K.M., Sutton, S.R., Fenter, P., Sturchio, N.C., Spötl, C., 2003. Uranyl incorporation in natural calcite. Environ. Sci. Technol. 37, 1284–1287.
Kelly, S.D., Rasbury, E.T., Chattopadhyay, S., Kropf, A.J., Kemner, K.M., 2006. Evidence of a stable uranyl site in ancient organic-rich calcite. Environ. Sci. Technol. 40, 2262–2268.
Keul, N., Langer, G., De Nooijer, L.J., Nehrke, G., Reichart, G.J., Bijma, J., 2013. Incorporation of uranium in benthic foraminiferal calcite reflects seawater carbonate ion concentration. Geochem. Geophys. Geosyst. 14, 102–111.
Kitano, Y., Oomori, T., 1971. The coprecipitation of uranium with calcium carbonate. J. Oceanogr. Soc. Jpn 27, 34–42.
Krantz, D.E., Jones, D.S., Williams, D.F., 1984. Growth rates of the sea scallop, Placopecten magellanicus, determined from the $^{18}O/^{16}O$ record in shell calcite. Biol. Bull. 167, 186–199.
Krestou, A., Panias, D., 2004. Uranium (VI) speciation diagrams in the $UO_2^{2+}/CO_3^{2-}/H_2O$ system at 25 °C. Eur. J. Miner. Process. Environ. 4, 113–129.
Ku, T., Luo, S., Lowenstein, T.K., Li, J., Spencer, R.J., 1998. U-series chronology of lacustrine deposits in Death Valley, California. Quat. Res. 50, 261–275.
Kulik, D.A., Vinograd, V.L., Paulsen, N., Winkler, B., 2010. $(Ca,Sr)CO_3$ aqueous-solid solution systems: from atomistic simulations to thermodynamic modelling. Phys. Chem. Earth 35, 217–232.
Kulik, D.A., Wagner, T., Dmytrieva, S.V., Kosakowski, G., Hingerl, F.F., Chudnenko, K.V., Berner, U.R., 2013. GEM-Selektor geochemical modeling package: revised algorithm and GEMS3K numerical kernel for coupled simulation codes. Comput. Geosci. 17, 1–24.
Lakshtanov, L.Z., Stipp, S.L.S., 2007. Experimental study of nickel(II) interaction with calcite: adsorption and coprecipitation. Geochim. Cosmochim. Acta 71, 3686–3697.
Lewis, E., Wallace, D., 1998. Program developed for CO_2 system calculations: Carbon Dioxide Information Analysis Center, Oak Ridge National Laboratory. U.S. Department of Energy.
Lorens, R.B., 1981. Sr, Cd, Mn and Co distribution coefficients in calcite as a function of calcite precipitation rate. Geochim. Cosmochim. Acta 45, 553–561.
Lundberg, J., Ford, D.C., 1994. Late Pleistocene sea level change in the Bahamas from mass spectrometric U-series dating of submerged speleothem. Quat. Sci. Rev. 13, 1–14.
Mavromatis, V., Gautier, Q., Bosc, O., Schott, J., 2013. Kinetics of Mg partition and Mg stable isotope fractionation during its incorporation in calcite. Geochim. Cosmochim. Acta 114, 188–203.
Meece, D.E., Benninger, L.K., 1993. The coprecipitation of Pu and other radionuclides with $CaCO_3$. Geochim. Cosmochim. Acta 57, 1447–1458.
Millero, F.J., 1995. Thermodynamics of the carbon dioxide system in the oceans. Geochim. Cosmochim. Acta 59, 661–677.
Min, G.R., Lawrence, E.R., Taylor, F.W., Recy, J., Gallup, C.D., Warren, B.J., 1995. Annual cycles of in coral skeletons and thermometry. Geochim. Cosmochim. Acta 59, 2025–2042.
Monteleone, B.D., Baldwin, S.L., Webb, L.E., Fitzgerald, P.G., Grove, M., Schmitt, A.K., 2007. Late Miocene-Pliocene eclogite facies metamorphism, D'Entrecasteaux Islands, SE Papua New Guinea. J. Metamorph. Geol. 25, 245–265.
Mucci, A., 1983. The solubility of calcite and aragonite in seawater at various salinities, temperatures, and one atmosphere total pressure. Am. J. Sci. 283, 780–799.
Owen, R., Kennedy, H., Richardson, C., 2002. Isotopic partitioning between scallop calcite and seawater: effect of shell growth rate. Geochim. Cosmochim. Acta 66, 1727–1737.
Paquette, J., Reeder, R.J., 1995. Relationship between surface structure, growth mechanism, and trace element incorporation in calcite. Geochim. Cosmochim. Acta 59, 735–749.
Raddatz, J., Liebetrau, V., Rüggeberg, A., Hathorne, E., Krabbenhöft, A., Eisenhauer, A., Böhm, F., Vollstaedt, H., Fietzke, J., Correa, M.L., Freiwald, A., Dullo, W., 2013. Stable Sr-isotope, Sr/Ca, Mg/Ca, Li/Ca and Mg/Li ratios in the scleractinian cold-water coral *Lophelia pertusa*. Chem. Geol. 352, 143–152.
Raitzsch, M., Kuhnert, H., Hathorne, E.C., Groeneveld, J., Bickert, T., 2011. U/Ca in benthic foraminifers: a proxy for the deep-sea carbonate saturation. Geochem. Geophys. Geosyst. 12.
Reeder, R.J., Nugent, M., Tait, C.D., Morris, D.E., Heald, S.M., Beck, K.M., Hess, W.P., Lanzirotti, A., 2001. Coprecipitation of uranium(VI) with calcite: XAFS, micro-XAS, and luminescence characterization. Geochim. Cosmochim. Acta 65, 3491–3503.
Russell, A.D., Emerson, S., Nelson, B.K., Erez, J., Lea, D.W., 1994. Uranium in foraminiferal calcite as a recorder of seawater uranium concentrations. Geochim. Cosmochim. Acta 58, 671–681.
Russell, A.D., Hönisch, B., Spero, H.J., Lea, D.W., 2004. Effects of seawater carbonate ion concentration and temperature on shell U, Mg, and Sr in cultured planktonic foraminifera. Geochim. Cosmochim. Acta 68, 4347–4361.
Sano, Y., Shirai, K., Takahata, N., Hirata, T., Sturchio, N.C., 2005. Nano-SIMS analysis of Mg, Sr, Ba and U in natural calcium carbonate. Anal. Sci. 21, 1091–1097.
Saulnier, S., Rollion-Bard, C., Vigier, N., Chaussidon, M., 2012. Mg isotope fractionation during calcite precipitation: an experimental study. Geochim. Cosmochim. Acta 91, 75–91.
Shimizu, N., Semet, M.P., Allègre, C.J., 1978. Geochemical applications of quantitative ion-microprobe analysis. Geochim. Cosmochim. Acta 42, 1321–1334.
Stipp, S.L., Hochella, M.F., Parks, G.A., Leckie, J.O., 1992. Cd^{2+} uptake by calcite, solid-state diffusion, and the formation of solid-solution: Interface processes observed with near-surface sensitive techniques (XPS, LEED, and AES). Geochim. Cosmochim. Acta 56, 1941–1954.
Stoll, H.M., Rosenthal, Y., Falkowski, P., 2002. Climate proxies from Sr/Ca of coccolith calcite: calibrations from continuous culture of *Emiliania huxleyi*. Geochim. Cosmochim. Acta 66, 927–936.
Sturchio, N.C., Antonio, M.R., Soderholm, L., Sutton, S.R., Brannon, J.C., 1998. Tetravalent uranium in calcite. Science 281, 971–973.
Tang, J., Köhler, S.J., Dietzel, M., 2008a. Sr^{2+}/Ca^{2+} and $^{44}Ca/^{40}Ca$ fractionation during inorganic calcite formation: I. Sr incorporation. Geochim. Cosmochim. Acta 72, 3718–3732.
Tang, J., Dietzel, M., Bohm, F., Köhler, S.J., Eisenhauer, A., 2008b. Sr^{2+}/Ca^{2+} and $^{44}Ca/^{40}Ca$ fractionation during inorganic calcite formation: II. Ca isotopes. Geochim. Cosmochim. Acta 72, 3733–3745.
Ter Kuile, B., Erez, J., 1984. In situ growth-rate experiments on the symbiont bearing foraminifera *Amphistegina lobifera* and *Amphistegina hemprichii*. J. Foraminifer. Res. 14, 262–276.
Tesoriero, A.J., Pankow, J.F., 1996. Solid solution partition of Sr^{2+}, Ba^{2+}, and Cd^{2+} to calcite. Geochim. Cosmochim. Acta 60, 1053–1063.
Thien, B., Kulik, D.A., Curti, E., 2014. A unified approach to model uptake kinetics of trace elements in complex aqueous - solid solution systems. Appl. Geochem. 41, 135–150.
Wagner, T., Kulik, D.A., Hingerl, F.F., Dmytrievava, S.V., 2012. Gem-selektor geochemical modeling package: TSolMod library and data interface for multicomponent phase models. Can. Mineral. 50, 1173–1195.
Watson, E.B., 1996. Surface enrichment and trace-element uptake during crystal growth. Geochim. Cosmochim. Acta 60, 5013–5020.
Watson, E.B., 2004. A conceptual model for near-surface kinetic controls on the trace- element and stable isotope composition of abiogenic calcite crystals. Geochim. Cosmochim. Acta 68, 1473–1488.
Watson, E.B., Liang, Y., 1995. A simple model for sector zoning in slowly grown crystals: implications for growth rate and lattice diffusion, with emphasis on accessory minerals in crustal rocks. Am. Mineral. 80, 1179–1187.
Winograd, I.J., Landwehr, J.M., Coplen, T.B., Sharp, W.D., Riggs, A.C., Ludwig, K.R., Kolesar, P.T., 2006. Devils Hole, Nevada, $\delta^{18}O$ record extended to the mid-Holocene. Quat. Res. 66, 202–212.
Wolthers, M., Nehrke, G., Gustafsson, J.P., Van Cappellen, P., 2012. Calcite growth kinetics: modeling the effect of solution stoichiometry. Geochim. Cosmochim. Acta 77, 121–134.